Elastic coupling between 90° twin walls and interfacial dislocations in epitaxial ferroelectric perovskites: A quantitative high-resolution transmission electron microscopy study

Ming-Wen Chu,[1,2,3,*] Izabela Szafraniak,[1,4] Dietrich Hesse,[1] Marin Alexe,[1] and Ulrich Gösele[1]
[1]*Max-Planck-Institut für Mikrostrukturphysik, Weinberg 2, D-06120 Halle (Saale), Germany*
[2]*Nanomaterials Laboratories, National Institute for Materials Science, 1-1 Namiki, Tsukuba, Ibaraki 305-0044, Japan*
[3]*Center for Condensed Matter Sciences, National Taiwan University, Taipei 106, Taiwan*
[4]*Institute of Materials Science and Engineering, Poznan University of Technology, M. Sklodowska Curie 5 Sq., 60-965 Poznan, Poland*
(Received 12 April 2005; revised manuscript received 31 August 2005; published 16 November 2005)

A quantitative high-resolution transmission electron microscopy study has been performed on tetragonal, single-crystalline $Pb(Zr_{0.4}Ti_{0.6})O_3$ islands grown on Nb-doped $SrTiO_3(001)$ substrates, revealing the strain fields of a 90° ferroelastic twin wall and the nearby interfacial dislocation. The twin wall, showing a width of ~1.5 nm and *compressive* strain features, is elastically coupled to the *tensile*-type strain of an edge dislocation having an out-of-plane Burgers vector, indicating an intimate interaction of the strain fields of both crystallographic defects. The long-range strain field of the dislocation core imposes a potential barrier on the twin wall, limiting its translational mobility under an applied electric field. The substrate clamping in the epitaxial island further acts as a restoring force on the electric-field-induced wall movement. The ensemble of these electromechanical boundary conditions thus indicates that the ferroelastic twin wall in the island should be immobile upon external electric fields. A further discussion also suggests that this complex interplay of the substrate clamping and the interfacial dislocation should account for the reported low twin-wall mobility in continuous, epitaxial ferroelectric perovskite films under an electric field.

DOI: 10.1103/PhysRevB.72.174112 PACS number(s): 61.72.Ff, 68.37.Lp, 77.80.Dj, 77.80.Fm

I. INTRODUCTION

Twins exist in a wide spectrum of crystalline materials, e.g., ferroelectrics, ferroelastics, and superconductors, relaxing the internal strain.[1] Interfacial dislocation networks appear in various epitaxial film and/or substrate heterostructures, accommodating the lattice misfit.[2–4] In bare ferroelectric perovskites such as $BaTiO_3$ and $Pb(Zr,Ti)O_3$, *static* 180° domains and 90° twins exist in the room-temperature ferroelectric phase, minimizing the energies of long-range electric and elastic fields correlated with the two respective order parameters, spontaneous polarization, and spontaneous strain, at the expense of the domain and twin wall energy.[3–9] While a 180° domain wall is ferroelectric with a negligible wall thickness, 90° twin walls exhibit a *ferroelastic* strain and possess a nonzero width and a considerable energy.[5–8]

Epitaxial thin-film ferroelectric perovskites have a high potential for advanced memory and electromechanical device applications due to the nonvolatility, remarkable electromechanical responses, and compositional and structural homogeneity.[2,10] Such heterostructures, in principle, involve interfacial dislocations.[2–8] The static structure of the epitaxial heterostructures thus represents an equilibrium between the 180° domains, 90° twins, and interfacial dislocations incorporated.[3–8,11] The ferroelastic twin walls in the films,[3,4,12] however, show low electric-field-induced translational displacements compared to those in the bulk.[13] Moreover, the field-driven wall mobility critically affects the electromechanical response of the devices.[10] Recent studies on the bare bulk materials with negligible charged defects (oxygen vacancies) suggest that the translational mobility of the twin walls is proportional to the wall width as a result of a narrow wall favoring a high lattice potential barrier that hinders the change in the order parameters within and crossing the wall.[1,6–8] By contrast, the low twin-wall mobility in thin films should be more related to the complex interplay of the intrinsic electromechanical boundary conditions imposed by the ferroelastic twin walls, the wall width, the interfacial dislocations, and the substrate clamping.[6–8,12–17] Although charged defects are suggested to accumulate on the twin walls both in bare bulk crystals and thin films, leading to the wall confinement, the role of this localized electrical boundary condition remains controversial.[18]

Recent attempts to reduce the influence of the substrate clamping by patterning epitaxial tetragonal $Pb(Zr,Ti)O_3$ films into discontinuous islands revealed an appreciable number of twin walls remaining electrically inactive.[17,19,20] The wall confinement mechanism in epitaxial ferroelectric perovskite films and islands, which could have electrical and/or structural origin, thus needs to be investigated in more detail. In this paper, we report the width of ~1.5 nm for a ferroelastic twin wall in epitaxial, tetragonal $Pb(Zr_{0.4}Ti_{0.6})O_3$ (PZT) islands and also present a possible structural origin for the confinement of the twin walls.

II. EXPERIMENT

We performed high-resolution transmission electron microscopy (HRTEM) investigations on epitaxial PZT islands crystallized at 800 °C on cubic Nb-doped $SrTiO_3(001)$ (STO) single-crystalline substrates that also serve as bottom electrodes. For details on growth conditions, see Ref. 21.

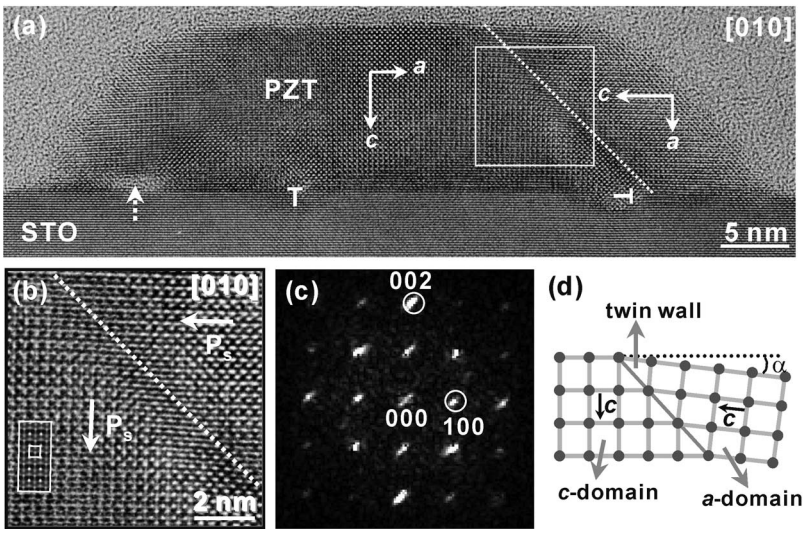

FIG. 1. (a) Cross-sectional HRTEM image of a PZT island in [010] zone axis. Dashed arrow, partial dislocation; **T**, edge dislocations; dashed line, 90° twin wall; square, twin-wall zone magnified in (b). (b) Magnified twin-wall region from (a). Dashed line, 90° twin wall; P_s, vector of the spontaneous polarization along the *c* axis; inset (bottom-left, rectangle), multislice image simulation at a crystal thickness of 1 nm and a defocus length of −65 nm; square in the inset, a PZT unit cell. At these imaging conditions, bright and gray (dark) contrasts represent the cation and anion columns, respectively. The better contrast towards the top-right corner is a sample thickness effect. (c) Power spectrum of (b). (d) Schematic representation of the twin-wall region. The angular deviation α from the orthogonality of the *c* axes and the lattice distortion around the twin wall are exaggerated for clarity.

HRTEM images taken on a JEOL 4010 electron microscope operated at 400 kV were digitized at a density of 0.041 nm/pixel. The nominal lattice parameters of tetragonal PZT and cubic STO are $a_{PZT}=3.985$ Å, $c_{PZT}=4.124$ Å, and $a_{STO}=3.905$ Å at room temperature.[22]

III. RESULTS AND DISCUSSION

A few of the grown PZT islands were observed to contain a twin wall. Figure 1(a) shows a cross-sectional HRTEM image of a PZT island in a [010] zone axis. A careful examination of Fig. 1(a) indicates a 90° twin wall in the PZT island (dashed line). Using multislice image calculations with the tetragonal *c* axis pointing to the substrate [inset in Fig. 1(b)], the fair agreement between the calculated and experimental contrasts reveals the epitaxial relationship $(001)_{PZT}[100]_{PZT}\|(001)_{STO}[100]_{STO}$ for the PZT region on the left of the wall, which is thus a *c* domain. The PZT region on the right of the wall is an *a* domain. Furthermore, the strain contrasts at the interface exhibit the presence of dislocations [Fig. 1(a)]. A Burgers circuit (not shown) indicates that the diffuse strain contrast on the left (dashed arrow) arises from a partial dislocation with a Burgers vector $\boldsymbol{b}=\frac{1}{2}a\langle 101\rangle$, cf., Ref. 23. The strain contrasts on the right and far right of the partial dislocation rather result from pure edge dislocations (indicated by **T**) with $\boldsymbol{b}=a\langle 100\rangle$ and $a\langle 001\rangle$, respectively, exhibiting the respective extra half-planes perpendicular and parallel to the interface [cf. Fig. 3(a)], both half-planes being on the STO side. An edge dislocation with the extra half-plane parallel to the interface has so far not been experimentally documented in detail.[2,11,23–25]

Figures 1(b) and 1(c) show an enlarged zone of the twin wall and the corresponding power spectrum, respectively. A zone relatively distant from the free surface and the neighboring dislocation was chosen to avoid contributions from structural information other than the wall. An investigation of Fig. 1(b) indicates the {101} wall orientation with a head-to-tail polarization configuration, suggesting a charge-neutral wall with negligible contributions from charged defects.[1,3,7] The ferroelastic strain $(c/a-1)\approx 3.5\%$ of the wall results in a calculated angular separation $\alpha=[2\arctan(c/a)-90°]\approx 2°$ between the two nominally orthogonal polar *c* axes [Figs. 1(b) and 1(d)].[1] This strain gives rise to the characteristic reflection splitting in reciprocal space [Fig. 1(c)] and the distortion of the neighboring lattices [Figs. 1(b) and 1(d)]. Compared to the theoretical angular separation of $\alpha\approx 2°$, the smaller estimated value of $\sim 1°$ from Fig. 1(b) suggests that the ferroelastic strain should be affected by the collective effects of the substrate clamping and strain fields of the adjacent dislocation core. Nevertheless, one should be aware of the influence of thin TEM specimen relaxations, which may also play a role in the deviation from the theoretical α value.[26,27]

It is then important to determine the thickness of the ferroelastic twin wall considering the fact that a significant wall width favors a large electric-field-induced mobility.[1,6–8] In the presence of a non-negligible substrate clamping and a dislocation nearby the wall [Fig. 1(a)], the lattice distortion and the corresponding strain fields in the vicinity of the wall may be distributed inhomogeneously. Therefore, we characterized the wall width using a quantitative analysis of a HRTEM image, the geometric phase method.[2,28,29] This method is based on a Fourier-space analysis of the lattice-fringe displacements and capable of deriving long-range strain fields of crystallographic defects with an ultimate resolution better than 1 Å.[28,29]

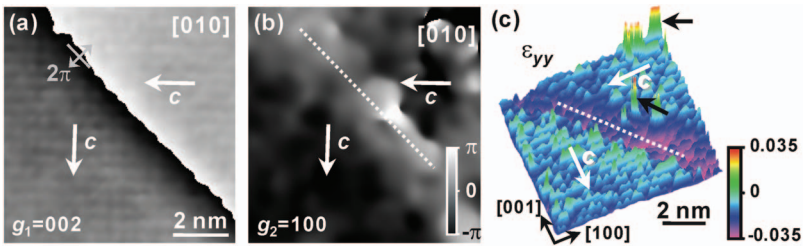

FIG. 2. (Color) (a) and (b) Geometric phase images corresponding to 1(b) calculated from the respective reciprocal-lattice vectors, $\boldsymbol{g}_1$ =[002] and $\boldsymbol{g}_2$=[100], indicated in 1(c). (a) and (b) show identical length and phase scales. The phase scale bar in (b) represents a normalization from $-\pi$ to π. (c) The associated out-of-plane strain field (ε_{yy}) of 1(b) using the geometric phase analysis along the [100] and [001] axes of (a). The black arrows show noise arising from loss in local contrast. The gray line in (a) and the dashed lines in (b) and (c) indicate the nominal wall.

The two reciprocal-lattice vectors $\boldsymbol{g}_1$ and $\boldsymbol{g}_2$ showing the best signal-to-noise ratio in Fig. 1(c) are $\boldsymbol{g}_1$=[002] and $\boldsymbol{g}_2$ =[100]. They were used to calculate the respective geometric phase images, Figs. 2(a) and 2(b), exploiting Gaussian masks and taking the undisturbed PZT lattice in the *c*-domain as the reference lattice.[2] The out-of-plane measure [Fig. 2(a)] indicates a sharp geometric-phase gradient with a period of 2π, i.e., a lattice periodicity along the *c* axis of the *c* domain of ~4 Å in real space, peaking at the nominal position of the wall. This gradient of 2π originates from the normalization of two separate gradients of $\sim\pi$ obtained when approaching the wall from *a* and *c* domain sides, respectively, [Fig. 2(a)].[28] Furthermore, a bending-type offset of the (001) planes by ~2 Å, corresponding to $\sim\pi$, at the twin wall is observed [Fig. 1(b)]. In regions relatively distant from the wall [Fig. 2(a)], the rather uniform geometric phase indicates homogeneous out-of-plane lattice parameters for both the *a* and *c* domains, despite the faint gridlike contrast artificially induced by the Fourier-space calculations.[28] In Fig. 2(b), the fluctuating contrast of the *a* domain and the twin-wall region, compared to the fairly uniform contrast in the *c* domain, stems from an *in-plane* elastic accommodation of the misfit strain ($\delta \approx 5.6\%$) in the *a* domain.

The two-dimensional displacement field, $\boldsymbol{u}(\mathbf{r})$, in the area shown in Fig. 1(b) was determined using $\boldsymbol{u}(\mathbf{r}) = -(\frac{1}{2}\pi) \times [P_{g1}(\mathbf{r})\boldsymbol{a}_1 + P_{g2}(\mathbf{r})\boldsymbol{a}_2]$,[28,29] where $\mathbf{r}$ is the position in the image, $P_{g1}(\mathbf{r})$ and $P_{g2}(\mathbf{r})$ are Figs. 2(a) and 2(b), respectively, and $\boldsymbol{a}_1$ and $\boldsymbol{a}_2$ are the real-space counterparts of $\boldsymbol{g}_1$ and $\boldsymbol{g}_2$, i.e., [001] and [200], respectively. The local lattice-distortion gradient *e* is defined as $e_{xx} = \partial \boldsymbol{u}_x(\mathbf{r})/\partial x$, $e_{xy} = \partial \boldsymbol{u}_x(\mathbf{r})/\partial y$, $e_{yx} = \partial \boldsymbol{u}_y(\mathbf{r})/\partial x$, and $e_{yy} = \partial \boldsymbol{u}_y(\mathbf{r})/\partial y$,[29] where $\boldsymbol{u}_x(\mathbf{r})$ and $\boldsymbol{u}_y(\mathbf{r})$ are the *x* and *y* components of $\boldsymbol{u}(\mathbf{r})$, respectively. The symmetric terms of these *e* matrices give the biaxial strain field components, ε_{xx} (in-plane), ε_{xy} ($=\varepsilon_{yx}$, shear), and ε_{yy} (out-of-plane).[2,28] Figure 2(c) shows the thus-derived ε_{yy} image, corresponding to e_{yy} with $\boldsymbol{u}_y(\mathbf{r}) = -(\frac{1}{2}\pi)P_{g1}(\mathbf{r})$ and with [100] and [001] as the respective *x* and *y* components. The wavy strain contrast in both *a* and *c* domains in Fig. 2(c) mainly results from the gridlike contrast in Fig. 2(a). The in-plane ε_{xx} and shear $\varepsilon_{xy} = \varepsilon_{yx}$ components are not suitable for analysis due to their significant noise arising from the fluctuating contrast in $P_{g2}(\mathbf{r})$ [Fig. 2(b), $\boldsymbol{u}_x(\mathbf{r}) = -(1/\pi)P_{g2}(\mathbf{r})$]. In Fig. 2(c), the wall region exhibits a *compressive* area embedded in a relatively strain-free surrounding. Considering the twin-wall region terminating at the compressive-strain cutoff [Fig. 2(c)], a wall width of 1.5±0.2 nm is obtained. Moreover, the broad width observed close to the neighboring dislocation (towards the bottom-right corner) indicates an elastic influence of this line defect. It is also noted that the wall width of ~1.5 nm, close to ~4 unit cells, could be already significant enough that the associated lattice potential barrier, which can hinder the wall movement under an electric field, may be insignificant.[8]

It has been theoretically proposed that the domain wall, being a transition region for order parameters, should involve internal strain,[30,31] and that it is feasible to consider the onset of the unstrained lattice region as the boundary of the wall.[30] Indeed, the change of the atomic structure inside the domain wall [Fig. 1(b)], mediating the transition of the order parameters, is correlated with the compressive strain characterized [Fig. 2(c)]. Moreover, the thus-determined wall width of ~1.5 nm in PZT is at the lower limit of the reported wall thickness of 4–10 lattice parameters, i.e., ~1.6~4 nm, in $BaTiO_3$ and $Pb(Zr_{0.52}Ti_{0.48})O_3$ microcrystalline ceramics.[27] The rather wider walls in the ceramics[27] could be ascribed to the fact that the twin wall width is sensitive to the atomic structure, i.e., to the strain, inside the wall.[17,30,31] Both first-principles and Landau-thermodynamics calculations of the twin wall width in tetragonal ferroelectric perovskites with a

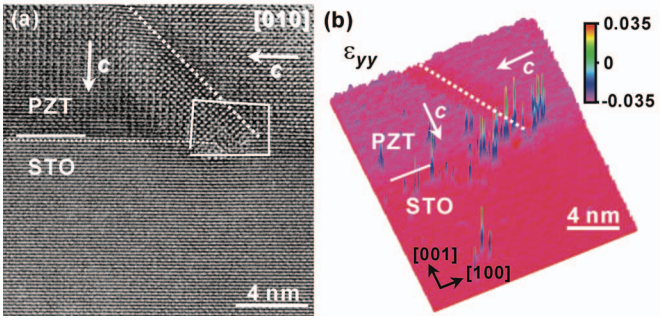

FIG. 3. (Color) (a) Enlarged HRTEM image from 1(a) revealing contrasts in the vicinity of the twin wall (dashed line) and the dislocation core with $\boldsymbol{b} = a\langle 001 \rangle$ indicated by the Burgers circuit. The dotted line shows the extra half TiO_2 plane on the STO side and the solid line indicates the interface. (b) The corresponding out-of-plane strain field (ε_{yy}) using the geometric phase analysis along the [100] and [001] axes of the geometric phase image with $\boldsymbol{g}_{1STO}$=[002] (see the text).

first-order phase transition suggest that the equilibrium wall thickness is below four lattice repeat distances, i.e., ~1.6 nm.[14,30] Furthermore, the change in atomic structure inside the wall is characterized by a local orthorhombic distortion.[30] In Fig. 1(b), the significant lattice distortion inside the PZT twin wall can, indeed, only be described by a symmetry lower than tetragonal. This fair agreement then implies that the ~1.5-nm-thick wall in the epitaxial PZT island could be close to the intrinsic wall thickness in the material. By contrast, the appreciable twin-wall thickness in $BaTiO_3$ and $Pb(Zr_{0.52}Ti_{0.48})O_3$ microcrystalline ceramics[13,27] may be an effect of the complex mechanical boundary conditions in the samples, e.g., grain boundaries and random grain orientations, which could affect the atomic structure and even the order of phase transition inside the wall.[5,8]

Figure 3(a), an enlarged zone of Fig. 1(a), shows part of the ferroelastic twin wall, the edge dislocation with $\boldsymbol{b} = a\langle 001\rangle$, and the TiO_2 extra half-plane in STO (dotted line). The out-of-plane strain field ε_{yy} [Fig. 3(b), estimated resolution of about 1 unit cell] in the area shown in Fig. 3(a) was derived by taking STO as the reference lattice due to the localization of the strain contrast on the STO side and by exploiting $\boldsymbol{g}_{1\mathrm{STO}}/\boldsymbol{g}_{2\mathrm{STO}}=[002]/[101]$ for the calculations. The globally low average in Fig. 3(b) is an artifact of the noisy experimental contrast of STO.[28] Nevertheless, the high average level in the *a* and *c* domains of PZT compared to that in STO indicates a fair measure of the strain along the [001] direction (nominally, $a_{\mathrm{PZT}}, c_{\mathrm{PZT}} > a_{\mathrm{STO}}$). The strain of *tensile* characteristics peaks in the vicinity of the dislocation [Fig. 3(b)]. More importantly, Fig. 3(b) reveals an intimate *elastic coupling* of the *compressive* strain of the twin wall to the *tensile* strain of the dislocation core with $\boldsymbol{b} = a\langle 001\rangle$.

Note that there exists a thermodynamic driving force to preferentially stabilize *c* domains on the conductive STO substrate taking into account the electric boundary condition correlated with STO and the respective misfit strain of *c* domains ($\delta \approx 2.1\%$) and *a* domains ($\delta \approx 5.6\%$).[5,6] The formation of *a* domains in the current case could then arise from the requirement to minimize the total energy attributed to long-range elastic, electrostatic, interfacial, and surface contributions.[8,15] At the growth temperature of 800 °C,[2,21] misfit dislocations were generated at the interface and immobilized slightly below this temperature. With a cooling to room temperature, the PZT–STO misfit is, however, not invariant due to a continuous change in lattice parameters of PZT and STO.[22,23,26] The formation of the 90° ferroelastic twin in PZT with a charge-neutral wall could be then associated with the relaxation of this additional misfit strain and the related equilibrium with the electrostatic, interfacial, and surface energies. The indicated energies are governed by the electric dipoles, the dislocation network, and the small ratio of the lateral dimension to thickness of the island, respectively. Intriguingly, theoretical calculations based on the Landau expansion of spontaneous polarization and spontaneous strain in ferroelectric perovskite films suggest that edge-type dislocations behave as nucleation sites for 90° twins,[15] in fair agreement with the coupling of a twin wall to a dislocation core observed in Fig. 3(b) and in Ref. 25 (80-nm-thick $BaTiO_3$ films on $LaAlO_3$). This good correlation between theory and experiments suggests that the electrostatic and elastic energies are the dominant terms in the total energy,[5–8,15] and supports the twin formation in PZT islands serving as a complementary strain accommodation mechanism to the misfit dislocation generation at the growth temperature. Note also that the observed distance of ~2 nm between the twin wall and the dislocation core [Fig. 3(a)] is theoretically demonstrated to be a characteristic of the long-range interaction of the strain fields of twin walls and interfacial dislocations with an out-of-plane Burgers vector.[7] A direct linking of a twin wall to a dislocation core with an in-plane Burgers vector has also been reported experimentally[25] and theoretically[7,8] considering the interaction of the strain fields.

In Fig. 3(a), the observed twin configuration is in fair agreement with the theoretical prediction[15] that a *c* domain forms on the top of a dislocation with an out-of-plane Burgers vector component. In a larger field of view [Fig. 1(a)], no other twin walls are observed in the vicinity of the partial dislocation (dashed arrow) and of the dislocation with an in-plane Burgers vector (indicated by **T**), while theoretical calculations[15] propose that a *c* domain and an *a* domain should be present on the top of the respective dislocations. This characteristic suggests that the elastic energy relevant to the aforementioned additional misfit strain may not be as significant as to generate other twins in the system.

Considering all above, an intimate elastic coupling between the twin wall and the dislocation core in PZT islands is indeed evident and qualitatively minimizes the long-range electromechanical energy. It is thus reasonable to suggest that the dislocation core behaves as an energetically favorable site for the twin-wall formation. The slight deviation from the calculated α value [Fig. 1(d)] and the gentle broadening of wall width toward the dislocation core can, therefore, be understood as effects of the interaction of long-range strain fields of the twin wall and the dislocation core, while a contribution from the substrate clamping should not be ignored. Taking into account the static features elucidated above, now we discuss their potential impact on the *dynamical* characteristics of the PZT–STO heterostructure under external electric boundary conditions, i.e., the situation in actual device applications.

At an electric field perpendicular to the interface of the island, the electromechanical energy of the system can be minimized by a field-induced state consisting of a single *c* domain due to the smaller misfit strain.[7,8] Such a switched single-*c*-domain state has to be accomplished by removing the twin wall from the island through a field-induced translational movement of the wall. This field-driven movement is, however, difficult, since the long-range strain field of the interfacial dislocation imposes a potential barrier on the twin wall.[7,8] The substrate clamping further acts as a restoring force on the wall under an electric field.[5] The ensemble of these electromechanical boundary conditions thus refers to the difficulty in mobilizing the twin wall by applying electric fields. This feature could also explain why it is not possible to electrically activate all twin walls in epitaxial $Pb(Zr,Ti)O_3$ islands.[12,19,20] Moreover, theoretical calculations on epitaxial ferroelectric thin films with dislocations showing an out-of-plane Burgers vector reveal the same constraint mechanism

for twin-wall movements.[8] As a consequence, the low twin-wall mobility in epitaxial ferroelectric perovskite films[3,4] and islands[12,19,20] under an electric field should have an identical origin, which is the complex interplay of the intrinsic electromechanical boundary conditions correlated with the substrate clamping and the interfacial dislocation.

IV. CONCLUSION

Using a quantitative HRTEM investigation on PZT islands, a ferroelastic twin wall with a thickness of ~1.5 nm was characterized and a mechanism for the twin formation in the heterostructure was proposed. More importantly, an elastic coupling between the twin wall and the dislocation core with an out-of-plane Burgers vector was visualized, indicating an intimate interaction of the strain fields of both crystallographic defects. The dislocation core imposes a potential barrier on the field-induced wall motion, and the substrate clamping acts as a restoring force on the wall movement under external electric fields. As a consequence, the twin wall in the islands should thus not be electrically active. This complex interplay of intrinsic electromechanical boundary conditions also explains the low twin-wall mobility under an electric field, frequently observed in other ferroelectric perovskite islands and films.

ACKNOWLEDGMENTS

The authors thank Professor James F. Scott (Symetrix Centre for Ferroics, University of Cambridge, UK) for most helpful discussions, and Professor Li Chang (Department of Material Science and Engineering, National Chiao Tung University, Taiwan) for technical help in multislice simulations of a HRTEM image.

*Corresponding author. Email address: chumingwen@ntu.edu.tw

[1] D. Shilo, G. Ravichandran, and K. Bhattacharya, Nat. Mater. **3**, 463 (2004).
[2] M.-W. Chu, I. Szafraniak, R. Scholz, C. Harnagea, D. Hesse, M. Alexe, and U. Gösele, Nat. Mater. **3**, 87 (2004).
[3] J. S. Speck and W. Pompe, J. Appl. Phys. **76**, 466 (1994).
[4] J. S. Speck, A. Seifert, W. Pompe, and R. Ramesh, J. Appl. Phys. **76**, 477 (1994).
[5] N. A. Pertsev, G. Arlt, and A. G. Zembilgotov, Phys. Rev. Lett. **76**, 1364 (1996).
[6] A. Yu. Emelyanov, N. A. Pertsev, and E. K. H. Salje, J. Appl. Phys. **89**, 1355 (2001).
[7] A. Yu. Emelyanov and N. A. Pertsev, Integr. Ferroelectr. **32**, 343 (2001).
[8] A. Yu. Emelyanov and N. A. Pertsev, Phys. Rev. B **68**, 214103 (2003).
[9] D. D. Fong, G. B. Stephenson, S. K. Streiffer, J. A. Eastman, O. Auciello, P. H. Fuoss, and C. Thompson, Science **304**, 1650 (2004).
[10] J. F. Scott, *Ferroelectric Memories* (Springer-Verlag, Berlin, 2000).
[11] S. Stemmer, S. K. Streiffer, F. Ernst, M. Rühle, W.-Y. Hsu, and R. Raj, Solid State Ionics **75**, 43 (1995).
[12] V. Nagarajan, A. Roytburd, A. Stanishevsky, S. Prasertchoung, T. Zhao, L. Chen, J. Melngailis, O. Auciello, and R. Ramesh, Nat. Mater. **2**, 43 (2003).
[13] Z. Li, C. M. Foster, X.-H. Dai, X.-Z. Xu, S.-K. Chan, and D. J. Lam, J. Appl. Phys. **71**, 4481 (1992).
[14] B. Meyer and D. Vanderbilt, Phys. Rev. B **65**, 104111 (2002).
[15] S. Y. Hu, Y. L. Li, and L. Q. Chen, J. Appl. Phys. **94**, 2542 (2003).
[16] J. S. Speck, A. C. Daykin, S. Seifert, A. E. Romanov, and W. Pompe, J. Appl. Phys. **78**, 1696 (1995).
[17] J. Chrosch and E. K. H. Salje, J. Appl. Phys. **85**, 722 (1999).
[18] M.-W. Chu, M. Ganne, M. T. Caldes, E. Gautier, and L. Brohan, Phys. Rev. B **68**, 014102 (2003).
[19] K. S. Lee, Y. K. Kim, S. Baik, J. Kim, and I. S. Jung, Appl. Phys. Lett. **79**, 2444 (2001).
[20] S. Bühlmann, B. Dwir, J. Baborowski, and P. Muralt, Appl. Phys. Lett. **80**, 3195 (2002).
[21] I. Szafraniak, C. Harnagea, R. Scholz, S. Bhattacharyya, D. Hesse, and M. Alexe, Appl. Phys. Lett. **83**, 2211 (2003).
[22] K.-H. Hellwege (ed.), *Landolt-Börnstein: Numerical Data and Functional Relationships in Science and Technology* (Springer-Verlag, Berlin), Group III: Crystal and Solid State Physics 3, 427 (1969).
[23] S. Stemmer, S. K. Streiffer, F. Ernst, and M. Rühle, Phys. Status Solidi A **147**, 135 (1995).
[24] T. Suzuki, Y. Nishi, and M. Fujimoto, Philos. Mag. A **79**, 2461 (1999).
[25] Z. R. Dai, Z. L. Wang, X. F. Duan, and J. Zhang, Appl. Phys. Lett. **68**, 3093 (1996).
[26] S. Stemmer, S. K. Streiffer, F. Ernst, and M. Rühle, Philos. Mag. A **71**, 713 (1995).
[27] F. Tsai, V. Khiznichenko, and J. M. Cowley, Ultramicroscopy **45**, 55 (1992).
[28] M. J. Hÿtch, E. Snoeck, and R. Kilaas, Ultramicroscopy **74**, 131 (1998).
[29] M. J. Hÿtch, J.-L. Putaux, and J.-M. Pénisson, Nature (London) **423**, 270 (2003).
[30] W. Cao and L. E. Cross, Phys. Rev. B **44**, 5 (1991).
[31] W. T. Lee, E. K. H. Salje, and U. Bismayer, J. Appl. Phys. **93**, 9890 (2003).